GRAPHITE-FIBER ELASTIC CONSTANTS: DETERMINATION FROM ULTRASONIC MEASUREMENTS ON COMPOSITE MATERIALS

Subhendu Datta
Department of Mechanical Engineering and CIRES
University of Colorado
Boulder, Colorado 80309-0449

Hassel Ledbetter
Institute for Materials Science and Engineering
National Institute of Standards and Technology
Boulder, Colorado 80303-3328

Tetsuyuki Kyono
Composite Materials Laboratory
Toray Industries
Shiga 520, Japan

INTRODUCTION

We determined the complete five-component transverse-isotropic-symmetry elastic-constant tensor for two graphite fibers: high-strength/low-modulus and low-strength/high-modulus. We did this in two steps. First, we measured ultrasonically the complete elastic constants of a metal matrix with embedded uniaxial graphite fibers. Second, we did an inverse-modeling calculation to extract the fiber's elastic constants. This calculation requires three inputs: composite elastic constants, matrix elastic constants, and fiber-matrix phase geometry, principally the fiber volume fraction. We compare the results with those expected for a random quasiisotropic graphite aggregate and for a hypothetical graphite fiber with perfectly aligned basal planes.

Graphite possesses remarkable physical properties. For example, the within-basal-plane Young modulus equals 902 GPa, four times that of iron (212 GPa), and 80% of that of diamond (1141 GPa). Also, graphite exhibits strong physical-property anisotropy: the E_1/E_3 Young-modulus ratio equals 29.8. (Here, x_3 denotes axis perpendicular to basal plane and x_1 denotes any direction in basal plane, which is isotropic.)

The fiber's elastic constants provide a valuable material characterization; they provide information on basal-plane alignment. Also, they enter many practical problems such as internal strain (residual stress).

MATERIALS

We studied four materials produced from commercial fibers and alloys. The two fibers are categorized as high-strength/low modulus and low-strength/high modulus. The two matrices consisted of pure magnesium and

5056 aluminum alloy. For the fibers, the manufacturer reported Young moduli of 235 and 392 GPa and mass densities of 1.76 and 1.81 g/cm^3, respectively.

Composites were produced by a squeeze-casting method, where molten matrix metal infiltrates carbon-fiber bundles under high pressure. Carbon fibers were preformed with a polymer fugitive binder. Placed in a mold, the preform was heated to slightly below the matrix-metal melting temperature. The binder was burned away and the carbon fibers were preheated. Molten matrix metal was poured into the mold and pressed at 98 MPa before solidification. This pressure caused the molten metal to infiltrate the fiber bundles. After solidification, the composite was removed from the mold. Further fabrication details occur elsewhere [1].

Figure 1 shows a typical microstructure. Focusing, for the moment, on the low-modulus magnesium-matrix material, by Archimedes's method, we found a mass density of 1.771 g/cm^3. For a fiber volume fraction of 0.70, using 1.738 for magnesium, and 2.269 for graphite, we predict a mass density of 2.110 g/cm^3. Probably, the discrepancy arises from nonperfectly graphitized fibers. Indeed, the manufacturer's reported fiber density, 1.76, leads to a prediction of 1.753, within 1 percent of observed. If we assume a void-and-crack-free matrix, our results predict a fiber density of 1.79 g/cm^3, corresponding to a fiber-void fraction of 0.21.

For the magnesium matrix material, a sample was prepared similar to that described above for the composite. For the matrix material, we found an Archimedes-method mass density of 1.738 g/cm^3, close to the accepted value for pure magnesium: 1.737. Similarly, for the 5056-aluminum-alloy matrix material, we found a mass density of 2.652, as expected slightly below the accepted value for pure aluminum, 2.697. Table 1 shows the measured elastic constants for these two matrix materials. The notation is C_ℓ = longitudinal modulus, G = shear modulus, B = bulk modulus, E = Young modulus, ν = Poisson ratio.

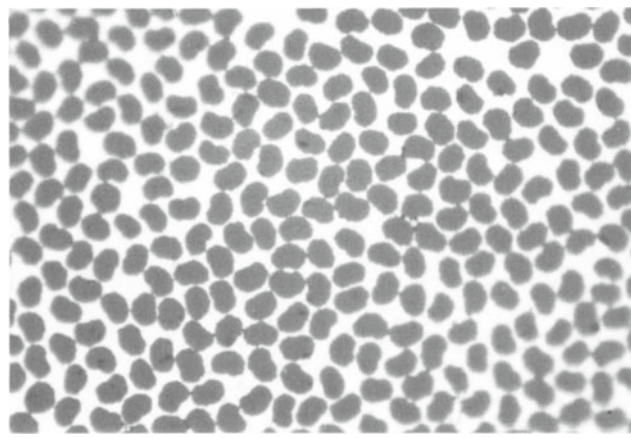

Fig. 1. Optical photomicrograph of transverse section of graphite-fiber-reinforced metal composite. The fibers, 7 μm in diameter, occupy 70 volume percent of the composite. All four studied composites show essentially the same microstructure. This case represents the low-modulus, aluminum-matrix case.

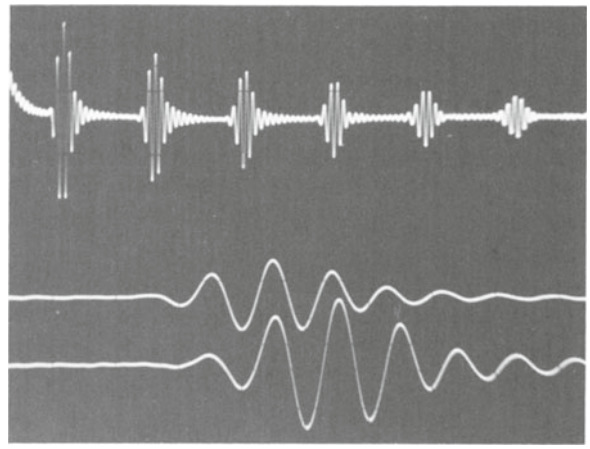

Fig. 2. Oscilloscope display of a pulse-echo pattern (top), expanded first echo (center), and expanded second echo (bottom). We measure transit time by superimposing the first nondistorted cycle of the first and second echoes. This example represents a longitudinal wave traveling parallel to the fibers.

Table 1. Elastic constants of matrix materials.

	C_ℓ (GPa)	G (GPa)	B (GPa)	E (GPa)	ν
Mg	57.88	17.72	34.26	45.34	0.279
Al alloy	109.40	26.22	74.45	70.39	0.342

Measurements

We determined the nine C_{ij} by measuring eighteen sound velocities on four specimen geometries described previously [2]. For brevity, we omit further description, except for a few salient details: bond—phenyl salicylate; transducers—quartz, x-cut and ac-cut; frequencies—5 to 6 MHz; specimen size—16-mm cube, or smaller depending on specimen geometry. Previously, we reported details of the measurement method [3]. Figure 2 shows an oscilloscope display.

Results

Table 2 shows principal results for one material: low-modulus fiber, magnesium matrix. Column 1 lists various elastic constants described in the previous section. Column 2 gives a set of graphite-fiber elastic constants [4]. We chose these because E_3 agrees closely with the E_3 for the present fiber. Column 3 gives elastic constants predicted by a theoretical model using the column-2 graphite-fiber elastic constants and the measured magnesium elastic constants.

Column 4 shows measured results: the nine orthotropic-symmetry C_{ij}, the principal Young moduli E_i, and the principal Poisson ratios ν_{ij}.

From the measured results and the above model, we calculated the graphite-fiber elastic constants, shown in column 5. We used the calculational sequence: C^f_{44}, C^f_{66}, $C^f_{11} - C^f_{66}$, ν^f_{31}, and E^f_3.

Column 6 shows the composite C_{ij} recalculated using the deduced C^f_{ij}. Finally, column 7 shows the ratio of column 6 to column 4, the ratio of recalculated to measured.

To calculate the predicted composite elastic constants shown in column 3, we used a model described elsewhere [5–7].

Table 2. Measured and calculated elastic constants for graphite-magnesium composite and calculated elastic constants for graphite fiber. Except for dimensionless ν_{ij}, units are GPa.

	Fiber[a]	Composite, Calculated	Composite, Measured	Fiber, Calculated	Composite, Recalc.	Ratio, Recalc. /Meas.
C_{11}	20.02	27.28	28.19	20.99	28.19	1.00
C_{22}	20.02	27.28	27.08	20.99	28.19	1.04
C_{33}	234.77	180.63	174.68	225.17	174.30	1.00
C_{44}	24.00	21.90	17.91	17.99	17.91	1.00
C_{55}	24.00	21.90	17.70	17.99	17.91	1.00
C_{66}	5.02	7.38	8.76	6.51	8.76	1.00
C_{12}	9.98	12.52	10.66	7.98	10.67	1.00
C_{13}	6.45	9.56	12.41	9.77	12.20	0.98
C_{23}	6.45	9.56	12.41	9.77	12.20	0.98
E_1	15.00	21.38	23.65	17.79	23.81	1.01
E_2	15.00	21.38	22.70	17.79	23.81	1.05
E_3	232.00	176.04	166.64	218.58	166.64	1.00
ν_{12}	0.494	0.449	0.374	0.367	0.359	0.96
ν_{13}	0.014	0.029	0.045	0.027	0.045	1.00
ν_{23}	0.014	0.029	0.046	0.027	0.045	0.98
ν_{21}	0.494	0.449	0.358	0.367	0.359	1.00
ν_{31}	0.215	0.240	0.314	0.337	0.314	1.00
ν_{32}	0.215	0.240	0.335	0.337	0.314	0.94

[a]Ref. 3.

Table 3 shows the deduced graphite-fiber elastic constants for all four cases. Table 3 also includes elastic constants for two useful reference cases: an aggregate of randomly oriented graphite crystals and a fiber where all the crystallite basal planes contain the fiber axis. For this latter case, we know only C_{33} and E_3 because the appropriate averaging problem remains unsolved.

Table 3. Deduced graphite-fiber elastic constants. Except for dimensionless ν_{ij}, units are GPa.

	Fiber 1		Fiber 2		Perfect Basal-plane Alignment	Quasi-isotropic Aggregate
	Al	Mg	Al	Mg		
C_{11}	19.09	20.99	11.24	12.58	-	160
C_{22}	19.09	20.99	11.24	12.58	-	160
C_{33}	234.99	225.17	348.89	361.45	1060	160
C_{44}	19.94	17.99	14.80	14.54	-	52
C_{55}	19.94	17.99	14.80	14.54	-	52
C_{66}	5.60	6.51	2.53	3.10	-	52
C_{12}	7.89	7.98	6.19	6.39	-	57
C_{13}	10.34	9.77	6.36	11.62	-	57
C_{23}	10.34	9.77	6.36	11.62	-	57
E_1	15.66	17.79	7.81	9.25	-	130
E_2	15.66	17.79	7.81	9.25	-	130
E_3	227.07	218.58	344.25	347.22	1020	130
ν_{12}	0.399	0.367	0.546	0.493	-	0.26
ν_{13}	0.026	0.027	0.008	0.016	-	0.26
ν_{23}	0.026	0.027	0.008	0.016	-	0.26
ν_{21}	0.399	0.367	0.546	0.493	-	0.26
ν_{31}	0.383	0.337	0.365	0.613	-	0.26
ν_{32}	0.383	0.337	0.365	0.613	-	0.26

Discussion

Results in column 4 of Table 2 show that the studied composite shows orthotropic elastic symmetry, which is approximately transversely isotropic, which requires four C_{ij} interrelationships:

$$C_{11} = C_{22};\ C_{13} = C_{23};\ C_{44} = C_{55};\ C_{66} = (C_{11} - C_{12})/2. \tag{1}$$

The microstructure in Fig. 1 also suggests transverse-isotropic symmetry.

Concerning the first-guess graphite-fiber elastic-constant calculations, we see good agreement for C_{11}, C_{22}, and C_{33}; fair agreement for C_{13} and C_{23}; and poor agreement for C_{44}, C_{55}, C_{66}, and C_{12}. Thus, the criterion of choosing a graphite-elastic-constant set based on E_3^f, the axial Young modulus, succeeds partially.

One can obtain a better, complete graphite-fiber elastic-constant set by using the model inversely. If we solve the usual model equations [4–9] for the fiber elastic constants, we obtain

$$C_{44}^f = \mu^m + \frac{2\mu^m(C_{44} - \mu^m)}{2c\mu^m - (1 - c)(C_{44} - \mu^m)}, \tag{2}$$

$$C_{66}^f = \mu^m + \frac{2\mu^m(C_{66} - \mu^m)(k^m + \mu^m)}{2c\mu^m(k^m + \mu^m) - (1 - c)(C_{66} - \mu^m)(k^m + 2\mu^m)}, \tag{3}$$

$$C_{11}^f - C_{66}^f = k^m + \frac{(k^m + \mu^m)(K - k^m)}{c(K + \mu^m) - (K - k^m)}, \tag{4}$$

$$\nu_{31}^f = \frac{\left(\frac{1 - c}{K^f} + \frac{c}{k^m} + \frac{1}{\mu^m}\right)\nu_{31} - (1 - c)\left(\frac{1}{K^f} + \frac{1}{\mu^m}\right)\nu^m}{c\left(\frac{1}{k^m} + \frac{1}{\mu^m}\right)}, \tag{5}$$

$$E_3^f = \frac{1}{c}[E_3 - (1 - c)E^m] - \frac{4(1 - c)(\nu_{31}^f - \nu^m)^2}{\frac{1 - c}{K^f} + \frac{c}{k^m} + \frac{1}{\mu^m}}. \tag{6}$$

From these five equations, the graphite-fiber elastic-constant results in column 5 of Table 2 differ significantly from the first-guess values in column 2. E_3^f is 3 percent lower than the first-guess value and 5 percent less than the fiber-manufacturer's estimate (235 GPa). Among all the calculated fiber-elastic-constant values, we have most confidence in E_3^f, which is well known to follow a linear rule-of-mixture. For the fibers (columns 2 and 5 in Table 1, the notable differences occur in the shear moduli: C_{44}^f and C_{55}^f differ by 25 percent and C_{66}^f by 30 percent. For transverse-isotropic symmetry, C_{44} is the torsional modulus T_3 around the x_3 axis—for fibers, an easily measured elastic constant. Thus, measuring T_3 and E_3 for fibers should provide useful information on fiber structure. That T_3 differs while E_3 is approximately the same suggests a structural difference not related to the orientation of hexagonal graphite unit cells in the fiber. We can compute the bulk modulus:

$$B = (2C_{11} + C_{33} + 2C_{12} + 4C_{13})/9. \tag{7}$$

For the first fiber we find 35.6 GPa, for the second 33.9 GPa. Reported graphite B values range from 34 to 210 GPa; and, from monocrystal measurements, theory predicts a possible range of 37 to 163 GPa [10]. Probably, the low B values for the present fibers reflect porosity or cracks.

After matching the graphite elastic constants to the measured composite elastic constants and recalculating the composite's properties, we should observe which composite C_{ij} constants differ most from observation. From Table 2, we see three: C_{22}, C_{13}, and C_{23}. C_{13} and C_{23} hardly surprise us because these indirect, off-diagonal elastic constants almost always present problems for both the experimentalist and the theorist. The other off-diagonal elastic constant presents little problem in the transverse-isotropic-symmetry case because of the relationship $C_{66} = (C_{11} - C_{12})/2$, where one can both measure and calculate C_{11} and C_{66} directly. The C_{22} disagreement arises because we assumed that an orthotropic-symmetry material was approximately transversely isotropic.

CONCLUSIONS

From this study, there emerged seven conclusions:

(1) Using ultrasonic methods usually applied to anisotropic monocrystals, we can determine the orthotropic (nine-component) elastic-constant tensor of a uniaxially fiber-reinforced metal-matrix composite.

(2) Although orthotropic, these particular composites show approximate transverse isotropy (five independent elastic constants).

(3) For a composite containing 70-volume-percent fibers, one can use a scattered-plane-wave ensemble-average model to describe and predict the composite's elastic constants.

(4) Graphite-fiber elastic constants chosen on the basis of the axial Young modulus, E_3, the most measurable fiber elastic constant, lead to wrong composite-elastic-constant predictions, especially for the shear moduli C_{ii} ($i = 4,5,6$).

(5) By knowing the matrix and composite elastic constants, and by using the model inversely, we can calculate the anisotropic fiber elastic constants.

(6) Graphite fibers with the same axial Young modulus, E_3, can possess different elastic constants, especially the torsional modulus $T_3 = C_{44}$.

(7) For all considered fibers, the bulk modulus computed from the C_{ij} lies near or below graphite's lower bound.

ACKNOWLEDGMENT

Specimens for study originated at the Toray Industries Composite Materials Laboratory in Otsu, Japan where we thank especially T. Kyono and A. Kitamura. Dr. R.D. Kriz provided the computer program. S.A. Kim made painstaking measurements. Ming Lei, guest worker from the Institute of Metal Research, Shenyang, P.R. China, provided some calculations and a critical reading. S.K. Datta received support from the Office of Naval Research, grant N00014-86-K-0280.

REFERENCES

1. A. Kitamura and S. Kataoka, in Proceedings, International Carbon Conference (Bordeaux, France, July 1984), p. 216. Toray Data Sheet TY-111A (June 1983).
2. H.M. Ledbetter and D.T. Read, J. Appl. Phys. 48, 1874–1879 (1977).
3. H.M. Ledbetter, N.V. Frederick, and M.W. Austin, J. Appl. Phys. 51, 305–309 (1980).
4. R.D. Kriz and W.W. Stinchcomb, J. Exper. Mech. 19, 41–49 (1979).
5. Z. Hashin and B.W. Rosen, J. Appl. Mech. 31, 223–232 (1964).
6. S.K. Bose and A.K. Mal, J. Mech. Phys. Solids 22, 217–229 (1974).
7. R. Hill, J. Mech. Phys. Solids 12, 199–212 (1964).
8. S.K. Datta and H.M. Ledbetter, Int. J. Solids Struct. 19, 885–894 (1983).
9. S.K. Datta, H.M. Ledbetter, and R.D. Kriz, Int. J. Solids Struc. 20, 429–432 (1984).
10. H.H. Wawra, B.K.D. Gairola, and E. Kröner, Z. Metallkd. 73, 69–71. (1982).